International Journal of
Environmental Research and Public Health

MDPI

Article

Adsorption Behavior and Relative Distribution of Cd^{2+} Adsorption Mechanisms by the Magnetic and Nonmagnetic Biochars Derived from Chicken Manure

Fei Huang [1,2,†], Lu Zhang [2,†], Ren-Ren Wu [3], Si-Ming Zhang [2] and Rong-Bo Xiao [1,*]

1 Guangdong Industrial Contaminated Site Remediation Technology and Equipment Engineering Research Center, School of Environmental Science and Engineering, Guangdong University of Technology, Guangzhou 510006, China; feihuang2011@163.com
2 College of Natural Resources and Environment, South China Agricultural University, Guangzhou 510642, China; xuml0916@163.com (L.Z.); bigchuang502@163.com (S.-M.Z.)
3 Guangdong Key Laboratory of Water and Air Pollution Control, South China Institute of Environmental Sciences, Ministry of Ecology and Environment, Guangzhou 510530, China; wurenren@scies.org
* Correspondence: ecoxiaorb@163.com
† The authors contributed equally to this study.

Received: 21 February 2020; Accepted: 26 February 2020; Published: 2 March 2020

Abstract: The present study investigated the adsorption of Cd^{2+} by nonmagnetic and magnetic biochars (CMB and M-CMB) derived from chicken manure, respectively. The adsorption characteristics were investigated as a function of initial pH, contact time, initial Cd^{2+} concentration and magnetic separation. Adsorption process of both biochars were better described by Pseudo-second-order kinetic equation and Freundlich isotherm model, which were spontaneous and endothermic in nature. It was found that maximum capacities were 60.69 and 41.07 mg/g obtained at the initial Cd^{2+} concentration of 180 mg/L for CMB and M-CMB, and the turbidity of adsorption-treated solution was reduced from 244.3 to 11.3 NTU after magnetic separation of 0.5 min. These indicated that M-CMB had lower adsorption capacity of Cd^{2+} than CMB, though it was successfully separated from the treated solutions. Furthermore, both biochars before and after adsorption were analyzed by SEM-EDS, XRD and FTIR. Adsorption mechanisms mainly included precipitation, ion-exchange, complexation and Cπ-coordination, in which precipitation and ion-exchange dominated the adsorption process by CMB, while in M-CMB, precipitation was always predominant mechanism, followed by ion-exchange. The two other mechanisms of complexation and Cπ-coordination were trivial in both biochars, jointly contributing 7.21% for CMB and 5.05% for M-CMB to total adsorption. The findings deepen our understanding of the mechanisms governing the adsorption process, which are also important for future practical applications in the removal of heavy metals from wastewater by the biochars.

Keywords: heavy metal; magnetic biochar; adsorption mechanism; magnetic separation; wastewater treatment

1. Introduction

Cadmium (Cd) is one of the most toxic heavy metal pollutants in wastewater, since it accumulates in living organisms and passes through the food chain into human organs, causing serious toxicity even at low concentration of 0.001–0.1 mg/L [1]. Significant quantities of Cd are introduced into the environment by anthropogenic activities, including manufacturing of nickel-cadmium batteries, synthetic pigment production, metal coatings, stabilizers in plastic products, and incineration of solid wastes, in which the worldwide production of Cd in 2005 was estimated to be 20,000 metric tons [2]. Accordingly, the adsorption using agricultural waste materials is one of the most popular and effective

processes for the removal of heavy metals from wastewater. Recently, the attention has been diverted towards the biochar that is obtained from the pyrolysis process of biomass including crop residues, manure and sewage sludge under low temperature (<700 °C) and oxygen-limited environment [3].

Among the biochars, magnetic biochar have been extensively used for heavy metal adsorption, since it could remove Cd^{2+} from aqueous solution to some extent and is easily separated from the wastewater [4]. For example, Li et al. [5] reported the synthesis of magnetic biochar by direct heating of siderite and rice husk under N_2 condition, and indicated that the adsorption capacity of U(VI) was significantly enhanced after magnetization. While Son et al. [6] developed an engineered magnetic biochar by pyrolyzing waste marine macro-alga, and found that the adsorption efficiency of heavy metal was partially reduced by magnetic biochar. These investigations and other studies [7–10] showed that the adsorption capacity of heavy metal by magnetic biochar, might be higher or lower than to that of nonmagnetic biochar. Therefore, it is necessary to evaluate the effect of magnetism loading on biochar in terms of the cationic heavy metal adsorption capacity, before a decision for the potential use of magnetic biochar as an industrial adsorbent is made.

The mechanisms responsible for Cd^{2+} adsorption by the biochars include: (i) precipitation with minerals (such as PO_4^{3-}, CO_3^{2-}, SiO_3^{2-}) [11,12]; (ii) exchange with cations (e.g., K^+, Ca^{2+}, Na^+, Mg^{2+}) [13,14]; (iii) surface complexation with oxygen-containing functional groups (e.g., −OH, −COOH, −R−OH) [15,16]; and (iv) coordination with Cπ electrons (e.g., C = C, C ≡ C) [13,17]. Among these mechanisms, Cui et al. [18] reported that the precipitation with minerals was the primary mechanism for Cd^{2+} adsorption on high-temperature biochars derived from *Canna indica*. Zhang et al. [12] showed that the Cd^{2+} adsorption primarily involved coordination with Cπ electrons in the biochar derived from *Phyllostachys pubescens*. Likewise, Wang et al. [16] indicated that Cπ-coordination was the predominant mechanism for Cd^{2+} adsorption by the biochars derived from bamboo, straw and pig manure. Despite the previous work, there is still a lack of existing literature on the comparison between magnetic and nonmagnetic biochar, focusing on the relative contribution of different mechanisms to total adsorption.

To summarize, the main objectives of the present study were to examine the adsorption characterization of Cd^{2+} by magnetic and nonmagnetic biochars derived from chicken manure, respectively, and to understand the contributions of each mechanism to total adsorption on a qualitative and quantitative basis by means of SEM-EDS, XRD and FTIR analysis.

2. Materials and Methods

2.1. Biochar Preparation and Characteristics

Chicken manure was collected from the farmland at South China Agricultural University, Guangzhou, China. The raw material was dried at 80 °C for 48 h until moisture was evaporated completely, and then sieved to <2.0 mm particles by a stainless grinding machine. For the synthesis of magnetic biochar (M-CMB), $FeCl_3{\cdot}6H_2O$ (20.0 g) and $FeSO_4{\cdot}7H_2O$ (11.1 g) was added to the beaker with 600 mL of deionized water and stirred until they were dissolved completely, after which the powdered biomass was mixed with the solutions and stirred at room temperature (25 ± 2 °C) for 20 min. Thereafter, 10 M-NaOH (aqueous) was added drop wise into the mixed suspension until the pH reached to 10–11. After being stirred for 30 min, the suspension was slowly pyrolyzed in a muffle furnace under N_2 atmosphere at 600 °C for 4 h according to the methods of Mohan et al. [19]. As a control, nonmagnetic biochar sample (CMB) was prepared under the same pyrolysis conditions, as previously described by Huang et al. [20].

The pH of biochar in water solution was determined at 1:20 (*w*/*v*) ratio after stirring for 1 h, and the content of ash was measured by heating at 800 °C for 4 h in a muffle furnace. To determine the point of zero charge (pHpzc), the zeta potential at various pH values was examined by a Zeta Meter (Malvern, Nano ZS90, UK). The BET surface area was measured by N_2 adsorption at liquid nitrogen temperature using a Gemini 2360 Micromeritics surface area analyzer and Brunauer-Emmett-Teller equation, and the content of C, H, O, N and S was determined by an elemental analyzer (Flash

EA1112, Thermo Finnigan, Italy). The minerals content of K, Ca, Na and Mg were determined by a flame atomic absorption spectrophotometer (FAAS) (M6, Termo Elemental, Waltham, MA, USA), respectively. The content of Fe and Cd in digestion solution were measured by inductively coupled plasma mass spectrometry (ICP-MS, Thermo Fisher Scientific, Waltham, MA, USA). The concentrations of water-soluble PO_4^{3-} and CO_3^{2-} were measured by ion chromatography (IC1000, Dionex Co., Ltd. Sunnyvale, CA, USA). The magnetic properties of biochar were determined by a comprehensive physical measurement system (PPMS-9, Quantum Design, San Diego, CA, USA).

2.2. Adsorption Experiments

Metal stock solutions of 1000 mg/L were prepared by dissolving $CdCl_2 \cdot 2.5H_2O$ (GR, guaranteed reagent) in double distilled water, and then diluted to the desired concentration prior to the adsorption experiments. Batch adsorption were performed by adding 0.03 g biochar samples to 30 mL synthetic solutions containing a known initial Cd^{2+} concentration at room temperature (25 ± 2 °C), and agitated at a speed of 150 rpm. The concentrations of ions including Na^+ and Cl^- were lower than the detection limits, and the initial pH of mixed solutions was adjusted to 6.01 ± 0.2 by 0.1 M NaOH or HCl. The effect of pH on the adsorption was investigated in range of 2.0–8.0, and carried out by mixing 1 g/L adsorbents at the initial Cd^{2+} concentration of 100 mg/L. For adsorption kinetics, biochar samples were mixed with synthetic water containing 20, 50, and 100 mg Cd^{2+}/L at pH 6.0, respectively, and the residual Cd^{2+} concentration was determined at various time intervals up to 360 min. After adsorption equilibrium, the final suspensions were centrifuged (8000 rpm, 10 min) and then filtered (0.22 μm Millipore filter), the supernatant was thus prepared to the measurement of Cd^{2+}. Likewise, adsorption isotherm experiments were carried out at initial Cd^{2+} concentrations in the range of 10–180 mg/L under the temperature of 293, 303 and 313 K, respectively. The magnetic separation of biochar particles from aqueous solution was investigated using a magnetic field of 0.5 T, according to the methods of Wang et al. [21].

Lagergren's pseudo-first-order equation (Equation (1)), and pseudo-second-order equation (Equation (2)) were used to fit the adsorption kinetics process. Langmuir (Equation (3)), and Freundlich (Equation (4)) isotherm equations were applied to model the experimental data. Adsorption thermodynamic (Equations (5) and (6)) was established by fixing free energy (ΔG^0), enthalpy (ΔH^0) and entropy (ΔS^0), according to the methods described by Milonjić [22].

$$q_t = q_e\left(1 - e^{-k_1 t}\right) \quad (1)$$

$$q_t = \frac{k_2 q_e^2 t}{1 + k_2 q_e t} \quad (2)$$

$$q_e = \frac{q_{max} K_L C_e}{1 + K_L C_e} \quad (3)$$

$$q_e = K_F C_e^{\frac{1}{n}} \quad (4)$$

$$\Delta G^0 = -RT\ln(\rho_\omega K_D) \quad (5)$$

$$\ln(\rho_\omega K_D) = \frac{\Delta S^0}{R} - \frac{\Delta H^0}{RT} \quad (6)$$

where q_e and q_t are the adsorption capacity at equilibrium and time t (mg/g), respectively. k_1 (l/min), and k_2 (g/mg min) are the rate constants corresponding to the respective kinetic model. Ce (mg/L) is the residual Cd^{2+} concentration at equilibrium, q_{max} (mg/g) is the maximum adsorption capacity, K_L (L/mg), K_F (L/g) and n are the rate constants corresponding to the respective isotherm model. ΔG^0 (kJ/mol), ΔS^0 (kJ/mol/K), and ΔH^0 (kJ/mol) represent the changes of Gibb's free energy, entropy and enthalpy, respectively. K_D (L/g) is the thermodynamic equilibrium constant (Langmuir isotherm constant) and ρ_w (g/L) is the water density. R (8.314 J/K/mol) is the gas constant and T (K) is absolute

temperature. In the case when K_D is given in L/mg, the constants of $\rho_w K_D$ can be easily recalculated to become dimensionless by multiplying it by 1,000,000 Milonjić [22].

2.3. The Contribution of Different Adsorption Mechanisms

Both biochars (CMB and M-CMB) were demineralized by rinsing with 1 M HCl and distilled water until the pH of liquid became constant, then untreated and demineralized biochars (0.03 g) were added into 30 mL solutions with a known initial Cd^{2+} concentration (100 mg/L) and without Cd^{2+}, respectively. After adsorption, the reduced amount of Cd^{2+} by the biochars before and after demineralization could be considered as the contribution of these removed minerals, because most minerals in the biochars were removed by the acid dipping procedure, but the surface oxygen-containing functional groups were not altered [12,23]. After the adsorption of untreated biochars (CMB and M-CMB), the cations including K^+, Na^+, Ca^{2+} and Mg^{2+} in the solution with and without Cd^{2+} were determined by ICP-MS. After that, a drop of pH before and after Cd^{2+} adsorption on both demineralized biochars was merely from the complexation with the oxygen-containing functional groups. In addition, the biochars loaded with and without Cd^{2+} were prepared for chemical analysis using scanning electron microscopy with energy dispersive X-ray spectroscopy (SEM-EDS, Hitachi, Japan), X-ray diffractometer (XRD-6000, Shimadzu, Japan) and fourier transform infrared spectroscopy (FTIR, PerkinElmer 2000, Waltham, WA, USA).

The adsorption capacity resulting from precipitation (Q_{pre}), ion-exchange (Q_{exc}), complexation (Q_{com}), Cπ-coordination ($Q_{c\pi}$) and total adsorption (Q_{ct}), were calculated by the modified methods of Gao et al. [1] and Wang et al. [23], respectively. The corresponding contribution percentage of each mechanism to total adsorption was determined by the Q_{pre}/Q_{ct}, Q_{exc}/Q_{ct}, Q_{com}/Q_{ct} and $Q_{c\pi}/Q_{ct}$ ratio.

(i) The adsorption capacity resulted from precipitation was calculated by the difference in the adsorption amount of Cd^{2+} between on untreated and demineralized biochars.

$$Q_{pre} = Q_{ct} - Q_{ca}{*}Y \quad (7)$$

where Q_{ca} is the adsorption capacity of demineralized biochars (mg/g), Y is the yield of demineralized biochar from original biochar.

(ii) The adsorption capacity attributed to ion-exchange was obtained by subtracting cations released in the 0 mg Cd^{2+}/L solution as background concentration from total released cations in the100 mg Cd^{2+}/L solution.

$$Q_{exc} = Q_k + Q_{Ca} + Q_{Na} + Q_{Mg} \quad (8)$$

where Q_k, Q_{Ca}, Q_{Na}, Q_{Mg} are the adsorbed Cd^{2+} by net release amount of K^+, Ca^{2+}, Na^+ and Mg^{2+} during the adsorption process, respectively (mg/g).

(iii) The adsorption capacity resulted from complexation was estimated by the difference in pH change before and after adsorption on the demineralized biochars.

$$Q_{com} = Q_{pH}{*}Y \quad (9)$$

where Q_{pH} is the adsorbed Cd^{2+} by complexation with oxygen-containing function groups on demineralized biochars (mg/g).

(iv) The adsorption capacity resulted from Cπ-coordination was calculated by subtracting the sum of Q_{pre}, Q_{exc} and Q_{com} from total adsorption capacity.

$$Q_{c\pi} = Q_{ct} - Q_{pre} - Q_{exc} - Q_{com} \quad (10)$$

2.4. Statistical Analysis

All adsorption experiments were conducted in triplicate, and the standard deviation was calculated by descriptive statistics. Data were statistically analyzed by one-way analysis of variance (ANOVA) at a 0.05 probability level using SPSS 18.0.

3. Results and Discussion

3.1. Biochar Properties

Both biochars were alkaline with high pH values (Table 1, 11.43 for CMB and 11.55 for M-CMB), suggesting that it would potentially remove heavy metals from acid mine drainage [24]. This was correlated to ash content, since the content of ash showed a positive correlation with the alkalinity of bicohar, as observed by many researchers [20,25,26]. High content of ash was also partly reflected by the SEM observations exhibiting many impurities on the surface of biochars (Figure 1). Moreover, the ash contained a large amount of alkaline mineral elements such as K, Ca, Na and Mg, as demonstrated by EDS and XRD results, which might begin to separate from the organic matrix during the pyrolysis process at high temperature (>300 °C), resulting in the increase of pH to strong basicity [25]. In addition, the surface area decreased from 25.56 m^2/g in CMB to 5.44 m^2/g in M-CMB, which could be attributed to the synthesis of magnetic biochar, causing many micropores were covered by the ash of M-CMB. Similar phenomenon was obtained in the previous work of some researchers reporting the reduction in the surface area after magnetization, because the Fe-containing particles reduced the surface area by filling micropores [6,10,27].

Compared with CMB, the elemental content of M-CMB including C, H, O, and N decreased obviously, resulting in the increase of atomic ratio of H/C and O/C (Table 1). This suggested the increase in abundance of oxygen-containing functional groups such as hydroxyl and carboxylic, which might be responsible for the Cd^{2+} adsorption by surface complexation or Cπ-coordination [15,28]. Additionally, CMB contained higher content of alkaline metal cations and soluble anions compared to M-CMB, which could play an important role in the Cd^{2+} adsorption by ion-exchange and precipitation, respectively [29,30].

After the magnetization, M-CMB showed ferromagnetic properties with the saturation magnetization (Ms) of 64.96 emu/g (Figure S1), which was higher than that of pure Fe_3O_4 materials (Ms = 58.94 emu/g) [21]. Coincidentally, the SEM-EDS results implied that the iron particles might aggregate to the surface of magnetic biochar (Figure 1B), which was indicated by the FTIR spectra observing the stretching vibrations of Fe-O (around 565 cm^{-1}) [31], and further confirmed by XRD pattern implying the formation of Fe_3O_4. These suggested that M-CMB presented a superior magnetic response, because of massive coverage of biochar surface by iron particles.

Table 1. The main properties of both biochars.

Biochar	pH	pH_{pzc}	Ash (%)	S_{BET} (m^2/g)	Fe (mg/g)	Magnetism (emu/g)	Elemental Content (%)					Atomic Ratio		Soluble Ions Content (mg/g)					
							C	H	O	N	S	H/C	O/C	K^+	Ca^{2+}	Na^+	Mg^{2+}	CO_3^{2-}	PO_4^{3-}
CMB	11.43	2.18	78.64	25.56	—	—	11.35	1.07	23.07	0.89	0.25	1.13	1.52	8.37	0.30	3.34	0.02	1.19	0.03
M-CMB	11.55	2.44	86.64	5.44	10.82	64.96	3.17	0.37	15.93	0.72	0.45	1.40	3.77	5.71	0.02	0.52	0.01	0.63	0.01

S_{BET} is the Brunauer-Emmett-Tell (BET) surface area, m^2/g. pH_{pzc} is the pH at which the surface charge of biochar is zero.

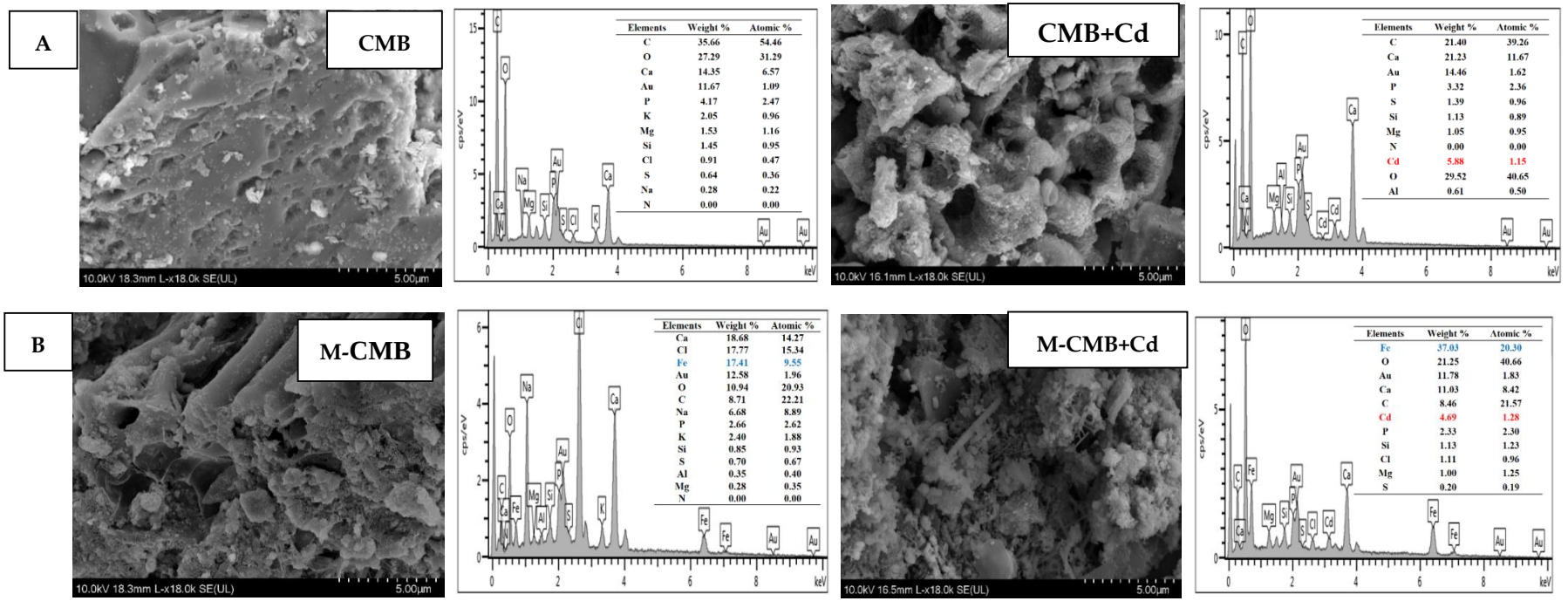

Figure 1. SEM images (left) and corresponding EDS spectra (right) of CMB (**A**) and M-CMB (**B**) before and after adsorption for Cd^{2+}.

3.2. Adsorption Characteristics

3.2.1. pH Adsorption Edge

Both adsorption capacities increased with increasing pH, and began to decline after reaching maximum adsorption at approximately pH 6.0, at which the maximum adsorption capacities were 51.37 mg/g for CMB and 28.30 mg/g for M-CMB, respectively (Figure 2A). The pH_{pzc} was calculated to be 2.18 and 2.44 for CMB and M-CMB, respectively (Figure 2B). When pH < pH_{pzc}, the surface charge of biochars became positive, causing electrostatic repulsion to positively charged Cd^{2+}, thus low level of adsorption was observed at pH 2.0 for both biochars. While pH > pH_{pzc}, the surface charge of biochars became negative, resulting in the significant increase of adsorption capacity from pH 2.0 to 6.0 [16]. Note that CMB showed higher adsorption capacities of Cd^{2+} than M-CMB, which may be due to the greater amount of negative charge, or larger of specific surface area of CMB compared to M-CMB under the pH range studied (Figure 2A,B). A similar phenomenon that the biochars have lower pH_{IEP} but higher adsorption capacity, was also reported in many previous works reporting that electrostatic interaction was likely the driving force for the Cd^{2+} adsorption onto biochar surfaces [1,32,33].

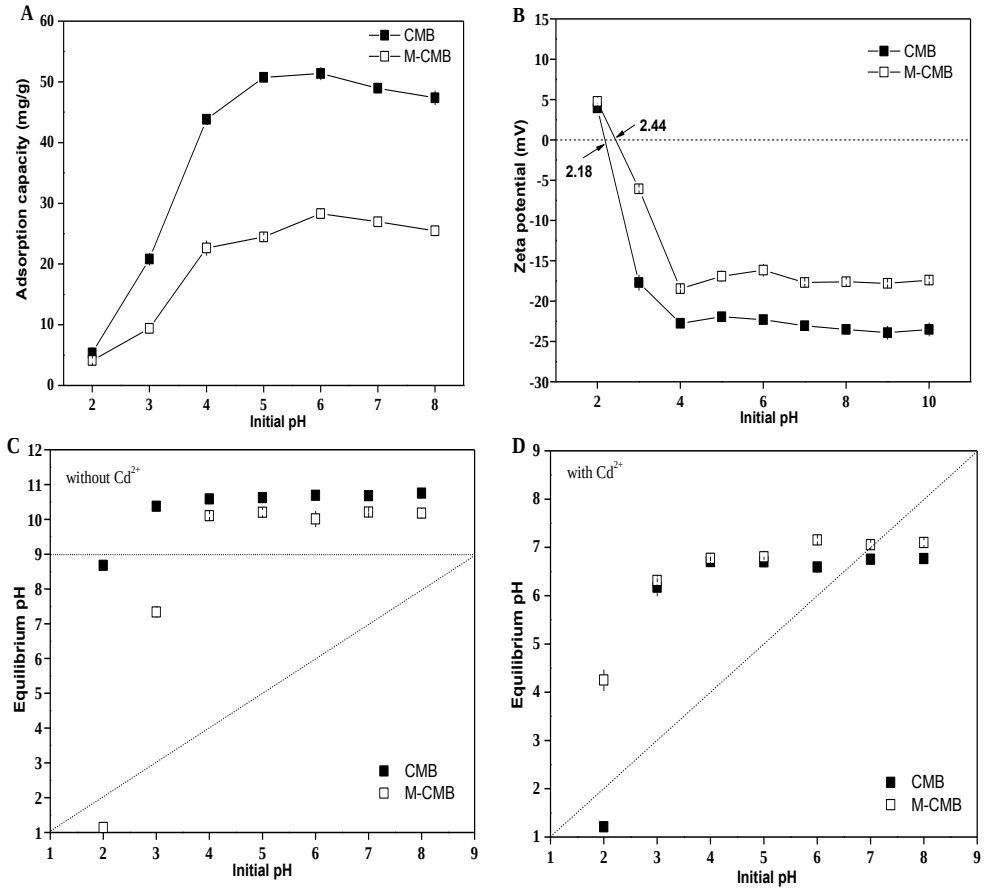

Figure 2. Effect of pH on the adsorption by both biochars (**A**). Zeta potential of both biochars at different initial pH values (**B**). Equilibrium pH of mixed solution without Cd^{2+} at different initial pH values (**C**). Equilibrium pH of mixed solution with Cd^{2+} at different initial pH values (**D**).

Compared with the initial pH, significant increase of equilibrium pH was observed for both biochars (Figure 2C), which was resulted from the addition of alkaline biochars to neutralize the solution acidity. Compared with the system without Cd^{2+}, equilibrium pH was lower when Cd^{2+} was adsorbed onto biochars (Figure 2C,D). This reduction could be attributed to surface complexation between Cd^{2+} and oxygen-containing functional groups such as −COOH and −OH, this was accompanied with the release H^+ into the solution, resulting in the decrease of equilibrium pH after adsorption [16,34].

Another explanation may be the formation of the Cd precipitate with PO_4^{3-} and CO_3^{2-}, reducing equilibrium pH after adsorption [18,20]. These observations suggested that electrostatic ion-exchange, complexation, and precipitation were involved in the adsorption process.

3.2.2. Adsorption Kinetics

Both adsorption generally exhibited initial high removal efficiency within 30 min, and then reached the equilibrium within almost 150 min (Figure 3). The adsorption capacities of CMB were 15.56 mg/g, 28.20 mg/g, and 37.97 mg/g within 150 min at initial Cd^{2+} concentrations of 20, 50 and 100 mg/L, accounting for 97%, 99%, and 97% to total capacity, respectively. In contrast, it seemed that the adsorption of M-CMB took longer to reach equilibrium, especially at the initial Cd^{2+} concentrations of 50 mg/L (Figure 3B). The adsorption capacities of M-CMB were much lower than those of CMB at the experimental conditions.

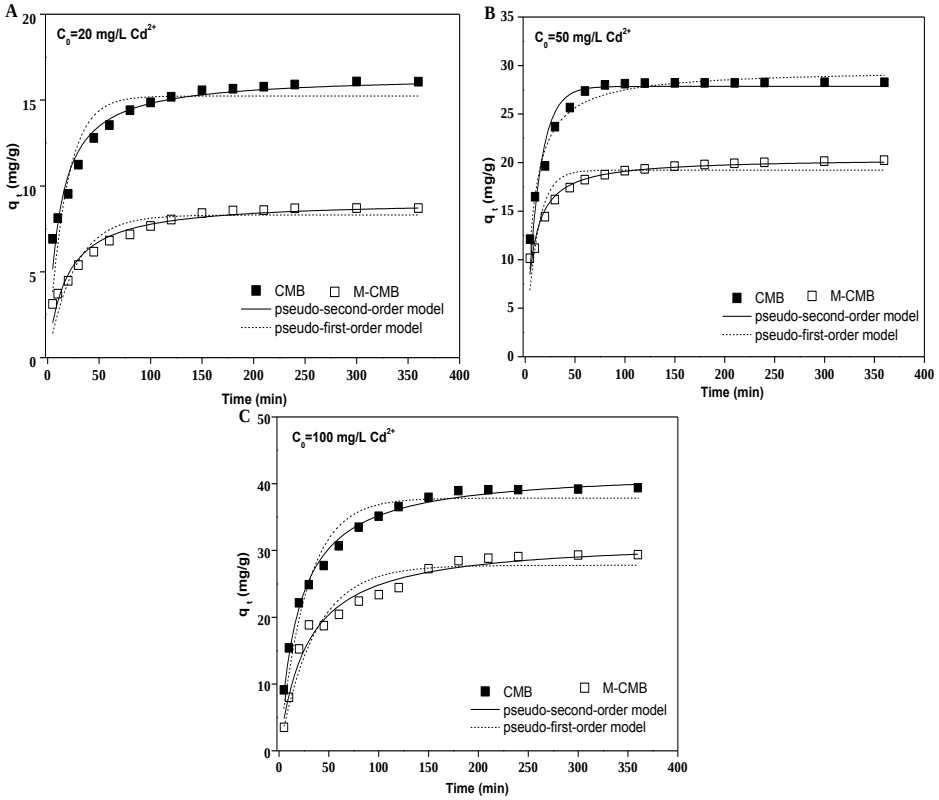

Figure 3. Effect of contact time on the adsorption at initial Cd^{2+} concentrations of 20 (**A**), 50 (**B**) and 100 mg/L (**C**), respectively.

Adsorption kinetics were assessed by pseudo-first-order and pseudo-second-order kinetic model, respectively (Figure 3). For both biochars, all the regression coefficients (R^2) of pseudo-second-order kinetic model were above 0.95, which were much larger than those of pseudo-first-order kinetic model (Table S1). Moreover, the adsorption capacities at equilibrium ($Q_{e,cal}$) calculated from pseudo-second-order kinetic model were very close to the experimental data ($Q_{e,\,exp}$). These indicated the adsorption followed the pseudo-second-order mechanism and corresponded to a chemisorption process [35]. In this regard, many studies indicated that the pseudo-second order model could predict almost all adsorption kinetic processes between metals and biomaterials, because of the basic on the adsorption capacity of solid adsorbents that forecasted the adsorption behavior over the entire process [36–38].

3.2.3. Adsorption Isotherms

Adsorption capacities increased rapidly with increasing initial Cd^{2+} concentration for both biochars, and leveled off approximately when the initial metal concentrations were above 120 mg/L in all cases (Figure 4A–C). These could be explained by a stronger driving force with increasing Cd^{2+} concentrations, leading to higher probability of collision between Cd^{2+} and biochars [39]. The maximum capacities were 42.44, 47.45 and 60.69 mg/g for CMB at the temperature of 293 K, 303 K, and 313 K, respectively. These were higher than those of M-CMB, with the respective maximum values of 29.32, 29.39, and 41.07 mg/g. Such difference in the adsorption capacities of both biochars was consistent with the results from adsorption kinetics (Figure 3) and pH adsorption edge (Figure 2), which were correlated with the different physico-chemical characteristics of both biochars.

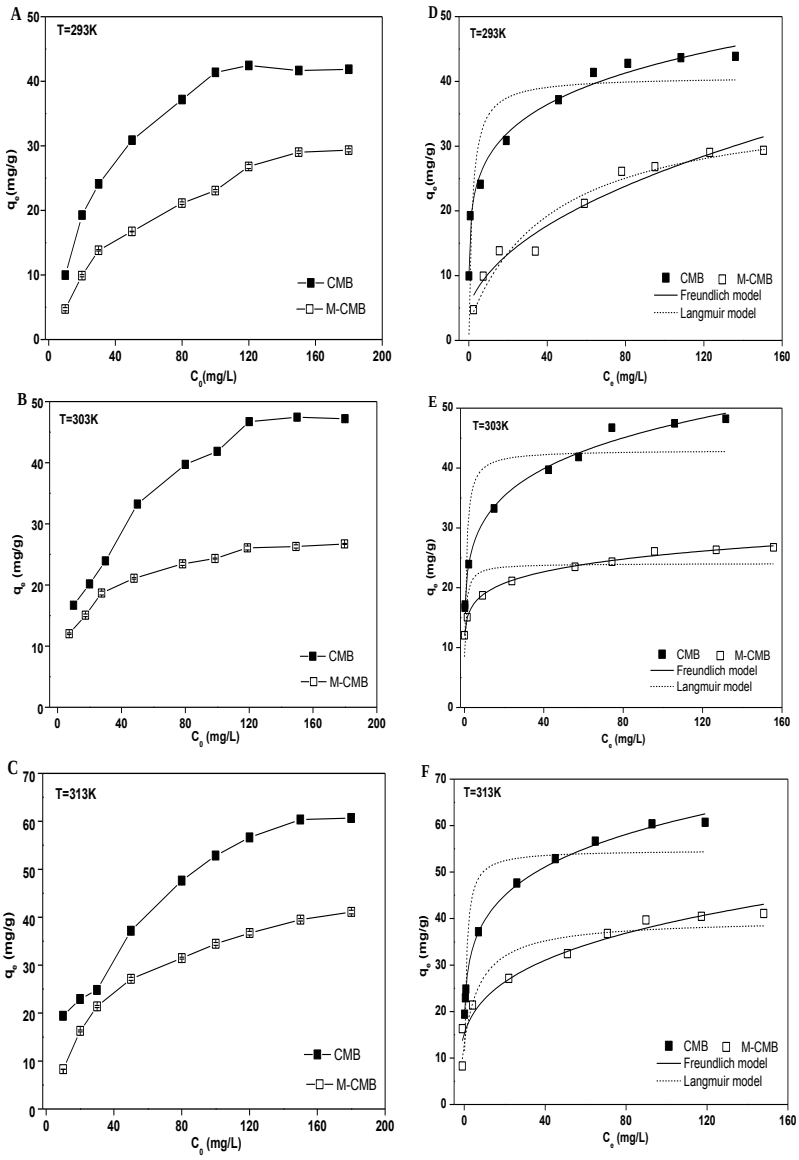

Figure 4. Effect of initial Cd^{2+} concentration on the adsorption under the temperature of 293 (**A**), 303 (**B**) and 313 K (**C**), respectively. Adsorption isotherms of the biochars under the temperature of 293 (**D**), 303 (**E**) and 313 K (**F**), respectively.

The experimental data were better fitted with the Freundlich isotherm than Langmuir isotherm under the temperature of 293 K, 303 K, and 313 K, respectively (Figure 4D–F). For both biochars, all the R^2 values of Freundlich model were greater than 0.95 (0.95–0.99), which were much higher than

those of Langmuir model (0.67–0.90). Meanwhile, all the 1/n values were observed in the ranges of 0.13–0.45 (Table S2), which satisfied the favorable adsorption condition ($0 < R_L < 1$) under the concentration ranges studied [35]. These indicated the chemisorption of Cd^{2+} onto both biochars had a great heterogeneity of adsorption affinity [40]. These results were in line with published data, describing that heavy metal adsorption were well fitted to Freundlich model by the magnetic biochars derived from rice husk [41], *loofah sponges* [42], and *chlorella vulgaris* [43].

3.2.4. Adsorption Thermodynamic

The adsorption process was spontaneous and endothermic in nature, with negative values of free energy (ΔG^0), positive values of enthalpy (ΔH^0) and entropy (ΔS^0) (Table 2). For both biochars, the negative values of ΔG^0 suggested that the spontaneous and feasible nature of adsorption process at all the studied temperatures. The negative values of ΔG^0 decreased as the rising temperature in CMB, implying the driving force to the adsorption increased with increasing temperature [44]. Meanwhile, the positive values of ΔH^0 highlighted the endothermic nature of adsorption by both biochars, and the positive values of ΔS^0 indicated randomness slightly increased during metal chemisopriotn from solution onto the surface of biochar [8,45].

Table 2. Thermodynamic parameters of adsorption for Cd^{2+} by both biochars.

Biochar	ΔG^0 (kJ mol^{-1})			ΔH^0 (kJ mol^{-1})	ΔS^0 (kJ mol^{-1} K^{-1})
	293 K	303 K	313 K		
CMB	−32.37	−35.63	−36.29	25.54	0.20
M-CMB	−25.11	−36.42	−31.63	73.05	0.34

3.2.5. Magnetic Separation of M-CMB

The turbidity of solution decreased from 244.3 to 11.3 NTU after magnetic separation within 0.5 min, whereas that of the one without magnetic field was 179.7 NTU (Figure 5). Moreover, the turbidity of solution kept relatively high (38.3 NTU) only by gravity after 50 min, while the magnetic separation rate was very rapid, owing to strong magnetism of M-CMB (Ms = 64.96 emu/g, Figure S1). These suggested that magnetic biochar particles could be successfully separated from the treated-solution with the help of external magnet.

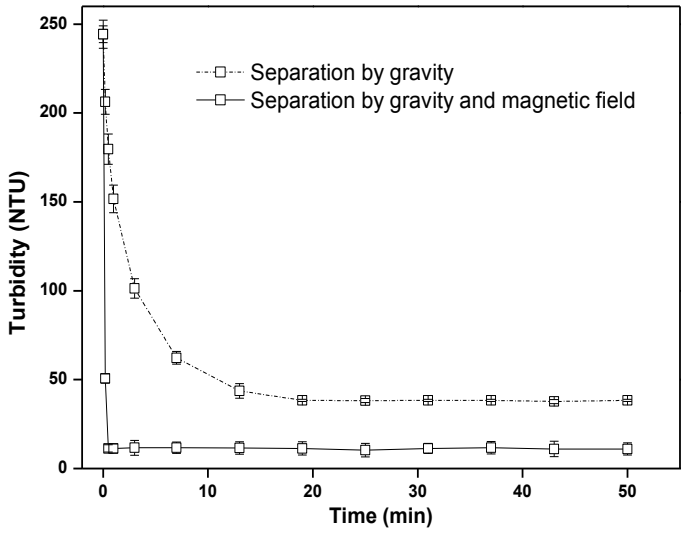

Figure 5. Effect of time on magnetic separation of M-CMB by a magnetic field of 0.5 T.

Combined with adsorption experimental data, it suggested that CMB had higher adsorption capacity of Cd^{2+} than that of M-CMB, this might be largely attributed to higher content of soluble ions for CMB, such as K^+, Ca^{2+}, Na^+, Mg^{2+}, CO_3^{2-} and PO_4^{3-} (Table 1), which was beneficial to the adsorption of Cd^{2+} through mixed mechanisms involving surface complexation, precipitation, ion-exchange, and Cπ-coordination. Similarly, the finding that the magnetization of biochar significantly reduced the adsorption efficiency, were also reported in the previous works, attributing it to the active sites of adsorbent being occupied by iron oxide particles [24,46].

3.3. Adsorption Mechanisms

3.3.1. Metal Precipitation

To confirm the role of precipitation, the untreated and Cd^{2+}-loaded biochars (150 mg/L) were scanned by XRD (Figure 6A). These precipitates on Cd-loaded biochars were possibly identified with typical peaks as $CdCO_3$, $Cd_3(PO_4)_2$, $CdSiO_3$, $Cd(OH)_2$, CdS, CdP_2, and $CdFe_2O_4$, although their presence cannot prove definitely. Coincidentally, some white granular crystals were visible on the biochars surface from the SEM observations (Figure 1), and their elemental composition mainly included Cd, C, O, P, S, Fe and Si, as indicated by EDS spectrum. This might partly support the occurrence of surface precipitation with minerals, or surface complexation with oxygen-containing functional groups [47]. The unfamiliar reduction state of P was detected as CdP_2 after adsorption, which might be resulted from the release of CH_4, H_2 and CO during pyrolysis [48]. Among these precipitates, such as $CdCO_3$, $Cd_3(PO_4)_2$, $CdSiO_3$, $Cd(OH)_2$ and CdS, were probably due to high concentrations of CO_3^{2-}, PO_4^{3-}, S and Si content in the original biochars (Figure 1 and Table 1), which were also observed in the previous studies on the heavy metal adsorption by the biochars [1,49,50]. In particular, the precipitates of $CdFe_2O_4$ were detected on the surface of M-CMB after adsorption, which could be attributed to the presence of Fe_3O_4 particles, generating adsorption sites for metal ions [6,10]. Generally, the intensities of XRD peak were strong in both biochars, suggesting the precipitation played an important role in total adsorption.

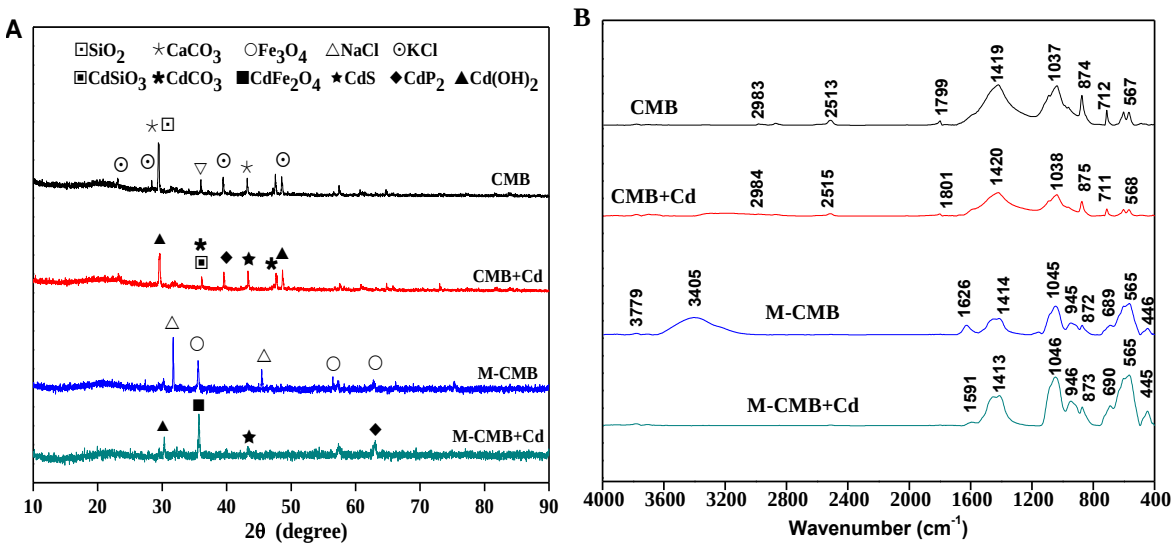

Figure 6. XRD patterns of both biochars before and after Cd^{2+} adsorption (**A**). FTIR spectra of both biochars before and after Cd^{2+} adsorption (**B**).

3.3.2. Surface Complexation

FTIR analysis was applied to characterize the changes of functional groups before and after adsorption (Figure 6B). For M-CMB, the peaks at 3779 cm^{-1} and 3405 cm^{-1} representing O-H vibrations of hydroxyl groups, were disappeared after interaction with Cd^{2+} [24]. The peak at 1626 cm^{-1} was

attributed to C = O stretching vibration of carboxyl, were significantly decreased after adsorption [47]. The band at 1414 cm^{-1} was assigned to CO_3^{2-} and the peak at 1045 cm^{-1} was due to P-O stretching vibrations of PO_4^{3-} [51], these were changed after adsorption, supporting the occurrence of the metal-carbonate and metal-phosphate precipitates, respectively (Figure 6A). Note that the bands between 880–780 cm^{-1}, 1100–1000 cm^{-1}, and 700–400 cm^{-1} were characteristic of Si-O-Si symmetric stretching, asymmetric stretching, and bending, respectively [52]. Considering that low content of Si in the original biochar (Figure 1), it would be more accurate to state that Si element probably participates in the adsorption by forming $CdSiO_3$, as partly supported by XRD analysis (Figure 6A). In particular, the peak at 446 cm^{-1} could be assigned to the stretching vibrations of Fe-O, testifying the formation of iron oxides [21]. In contrast, the bands of CMB at 2983 cm^{-1} (-CH stretching), 2513 cm^{-1} (CO_3^{2-}), 1799 cm^{-1}, 1037 cm^{-1} (P-O stretching vibrations of PO_4^{3-}), 874 cm^{-1} (Si-O-Si symmetric stretching), and 567 cm^{-1} (Si-O-Si bending) were all increased slightly after adsorption. These suggested that oxygen-containing functional groups such as -OH, -COOH, as well as C-H aromatic group might be involved in the adsorption. However, the intensities of FTIR spectra in both biochars changed slightly within 1–2 units, implying the complexation was an insignificant mechanism in total adsorption. Indeed, the adsorption capacity resulting from this mechanism were 2.13 mg/g and 1.26 mg/g for CMB and M-CMB, respectively (Table 3).

Table 3. Changes in hydrogen ion concentration of adsorption for Cd^{2+} by both biochars.

Biochar	Initial pH	Final pH	$\triangle H^+ (10^{-6}$ mmol)	Q_e (mg/g)
CMB	5.96 ± 0.02	3.87 ± 0.01	134 ± 0.06	2.13 ± 0.02
M-CMB	5.02 ± 0.01	4.36 ± 0.02	34.1 ± 0.18	1.26 ± 0.01

3.3.3. Cπ-Coordination

The cyclic aromatic π-system formed in the biochars could function as the π-donor in the Cd^{2+} adsorption [17]. According to the FTIR spectra (Figure 6B), the peaks between 900–700 cm^{-1} and 700–400 cm^{-1} representing the aromatic C-H groups changed slightly after adsorption, suggesting aromatic functional groups such as γ-CH of furan and β–ring of pyridine might be involved in the adsorption by both biochars [30]. These heterocyclic compounds were a weak cation-π binder and easily bind with Cd^{2+} by donating π electrons [53], it was thus reasonable to believe that the coordination with Cπ electrons would occur in the adsorption. Similar results were reported by Harvey et al. [13] and Machida et al. [54], who found that the heavy metal adsorption by biochars were mainly attributed to the coordination with delocalized π electrons from the functional groups such as γ-CH and C=C. The formation of Cd-Cπ bonds between Cd^{2+} and delocalized lone-pair π electrons could be described by the following reaction:

$$\diagdown\!\!\diagup C: + Cd^{2+} \rightleftharpoons \diagdown\!\!\diagup C: + Cd^{2+} \quad (11)$$

3.3.4. Ion-Exchange

Ion-exchange was considered as the dominant mechanism for heavy metal adsorption by the biochars [13,30]. In parallel with the Cd^{2+} adsorption, significant amount of K^+, Ca^{2+}, Na^+ and Mg^{2+} were released into the solution, equivalent to 22.75 and 8.01 mg Cd^{2+}/g (Table 4), accounting for 47.62% and 23.90% of total adsorption by CMB and M-CMB, respectively (Figure 7). These indicated that cation exchange played an important role in total adsorption. Moreover, the dominance of K^+ and Ca^{2+} among these released cations was observed in CMB, this was seemed fairly comparable to the

studies of Flores-Cano et al. [14] and Chen et al. [55], who proposed that Cd^{2+} substitution for Ca^{2+} was a major mechanism in the adsorption.

Table 4. The release of K^+, Ca^{2+}, Na^+ and Mg^{2+} during the Cd^{2+} adsorption by both biochars.

Biochar	The Net Amount of Released Cations (mequiv/g)				Sum	Overall Adsorbed Cd^{2+} (mg/g)
	K^+	Ca^{2+}	Na^+	Mg^{2+}		
CMB	14.43 ± 0.26	9.58 ± 0.38	7.10 ± 1.73	2.41 ± 0.07	33.52 ± 1.83	22.75 ± 0.88
M-CMB	7.90 ± 0.13	1.74 ± 0.08	4.11 ± 0.10	0.26 ± 0.02	14.01 ± 0.08	8.01 ± 0.06

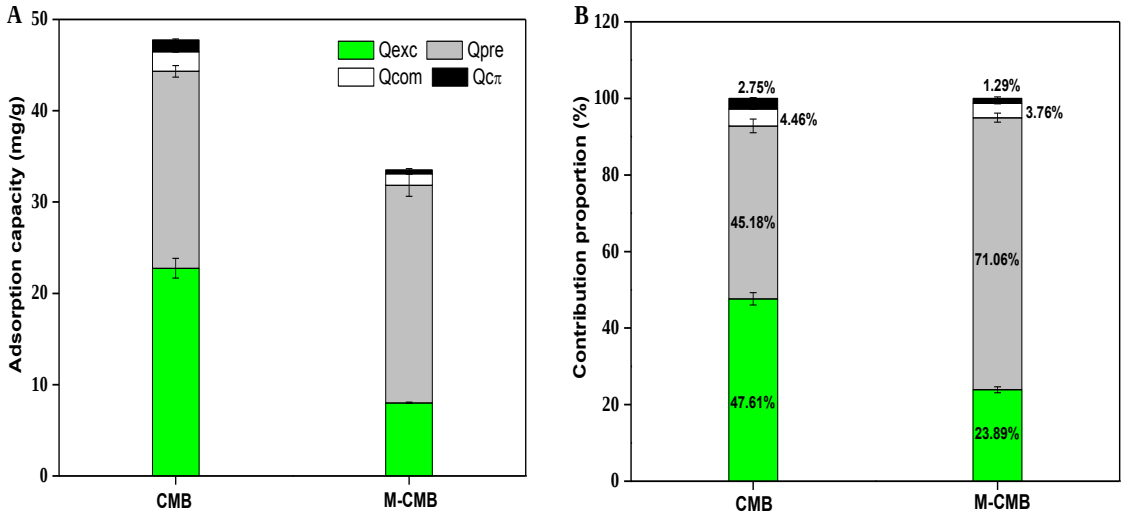

Figure 7. Adsorption capacity of Cd^{2+} adsorption by both biochars (**A**). Contribution percentage of different mechanisms to total adsorption by both biochars (**B**).

3.4. Relative Distribution of Adsorption Mechanisms

The precipitation formed the biggest fraction in M-CMB, because the Q_{pre} was 23.83 mg/g with relatively high contribution of 71.06% to total adsorption (Figure 7), highlighting that the precipitation was the dominant mechanism in total adsorption. While in CMB, the Q_{pre} was 21.57 mg/g, whose contribution proportion was 45.18% in total adsorption. Similar to the precipitation, ion-exchange produced the largest contribution to total adsorption for CMB (47.61%), though its importance was decreased slightly in M-CMB (23.89%). This situation seemed fairly comparable to the finding, in which the heavy metal adsorption by dairy-manure biochar was mainly attributed to the precipitation with PO_4^{3-} and CO_3^{2-} [51], and the adsorption by rice-straw biochar was closely related to the exchangeable cations [50], respectively. Thus, the precipitation and ion-exchange dominated the adsorption for both biochars, jointly contributing 92.79% in CMB and 94.95% in M-CMB to total adsorption. On the other hand, complexation and Cπ-coordination were comparably tiny among these mechanisms, since both Q_{com} and $Q_{c\pi}$ values were relatively low. The values of Q_{com} were 2.13 and 1.26 mg/g for CMB and M-CMB, with their corresponding contribution proportions were 4.46% and 3.76%, respectively. The $Q_{c\pi}$ values were 1.31 mg/g for CMB and 0.43 mg/g for M-CMB, whose contribution proportions were 2.75% and 1.29%, respectively.

Based on the present results, magnetic biochar like M-CMB should be further modified to enhance its adsorption ability for heavy metal ions. As a result, a variety of approaches would be applied to improve the adsorption ability of magnetic biochar, such as oxidation [56], amination [46] and loading of metal nanoparticles [57]. Among these methods, more efforts should be paid to explore the effect of new functional groups-impregnated magnetic biochar after modification, since there is a great potential in the enhancement of adsorption capacity for M-CMB, mainly by improving complexation and Cπ-coordination.

4. Conclusions

Compared with the M-CMB, CMB have greater adsorption capacities, faster adsorption kinetics, but have difficulties in separating from the solution after adsorption. For both biochars, the adsorption process followed chemisorption mechanism, occurring on the heterogeneous surface at tested conditions. Among the four mechanisms, the precipitation and ion-exchange dominated the adsorption, in combination contributing 92.79% for CMB and 94.95% for M-CMB, but complexation and coordination were comparably tiny in total adsorption. These could help to improve the application of biochar in environmental remediation for heavy metal. However, the research regarding the enhancement of adsorption capacity by magnetic biochar should be further investigated in future.

Supplementary Materials: The following are available online at http://www.mdpi.com/1660-4601/17/5/1602/s1, Fig. S1. Magnetization curves of M-CMB at room temperature. Table S1. Kinetic parameters of adsorption for Cd^{2+} by both biochars at different initial metal concentrations. Table S2. Isotherm parameters of adsorption for Cd^{2+} by both biochars at different temperatures.

Author Contributions: R.-B.X. conceived and designed the ideas to develop in the article; F.H. analyzed data and wrote the manuscript with help of L.Z., R.-R.W. provided the experimental sets; S.-M.Z. contributed in editing the manuscript. All authors contributed to the final version of this manuscript.

Funding: This research was financially supported by the National Key Research and Development Program of China (2017YFD0801000), National Natural Science Foundation of China (41977116), Key-Area Research and Development Program of Guangdong Province (2019B110207001), Basic and Applied Research Program of Guangdong Province (2019A1515012187), and the Key Laboratory of Water and Air Pollution Control of Guangdong Province (2017A030314001).

Conflicts of Interest: The authors declare that they have no competing financial interests.

References

1. Gao, L.Y.; Deng, J.H.; Huang, G.F.; Li, K.; Cai, K.Z.; Liu, Y.; Huang, F. Relative distribution of Cd^{2+} adsorption mechanisms on biochars derived from rice straw and sewage sludge. *Bioresour. Technol.* **2019**, *272*, 114–122. [CrossRef] [PubMed]
2. Joseph, P. Mechanisms of cadmium carcinogenesis. *Toxicol. Appl. Pharm.* **2009**, *238*, 272–279. [CrossRef] [PubMed]
3. Lehmann, J.; Joseph, S. *Biochar for Environmental Management: Science and Technology*; Earthscan: London, UK, 2009.
4. Yi, Y.; Huang, Z.; Lu, B.; Xian, J.; Tsang, P.E.; Wen, C.; Fang, J.; Fang, Z. Magnetic biochar for environmental remediation: A review. *Bioresour. Technol.* **2019**, *298*, 122468. [CrossRef] [PubMed]
5. Li, M.; Liu, H.; Chen, T.; Dong, C.; Sun, Y. Synthesis of magnetic biochar composites for enhanced uranium(VI) adsorption. *Sci. Total Environ.* **2019**, *651*, 1020–1028. [CrossRef] [PubMed]
6. Son, E.B.; Poo, K.M.; Chang, J.S.; Chae, K.J. Heavy metal removal from aqueous solutions using engineered magnetic biochars derived from waste marine macro-algal biomass. *Sci. Total Environ.* **2018**, *615*, 161–168. [CrossRef] [PubMed]
7. Li, M.; Wei, D.; Liu, T.; Liu, Y.; Yan, L.; Wei, Q.; Du, B.; Xu, W. EDTA functionalized magnetic biochar for Pb(II) removal: Adsorption performance, mechanism and SVM model prediction. *Sep. Purif. Technol.* **2019**, *227*, 115696. [CrossRef]
8. Navarathna, C.M.; Karunanayake, A.G.; Gunatilake, S.R.; Pittman Jr, C.U.; Perez, F.; Mohan, D.; Mlsna, T. Removal of Arsenic(III) from water using magnetite precipitated onto Douglas fit biochar. *J. Environ. Manag.* **2019**, *250*, 109429. [CrossRef]
9. Zhao, Y.; Zhang, R.; Liu, H.; Li, M.; Chen TChen, D.; Zou, X.; Frost, R.L. Green preparation of magnetic biochar for the effective accumulation of Pb(II): Performance and mechanism. *Chem. Eng. J.* **2019**, *375*, 122011. [CrossRef]
10. Wang, X.; Xu, J.; Liu, J.; Liu, J.; Xia, F.; Wang, C.; Dahlgren, R.A.; Liu, W. Mechanism of Cr(VI) removal by magnetic greigite/biochar composites. *Sci. Total Environ.* **2020**, *700*, 134414. [CrossRef]

11. Inyang, M.; Gao, B.; Yao, Y.; Xue, Y.; Zimmerman, A.R.; Pullammanappallil, P.; Cao, X. Removal of heavy metals from aqueous solution by biochars derived from anaerobically digested biomass. *Bioresour. Technol.* **2012**, *110*, 50–56. [CrossRef]
12. Zhang, C.; Shan, B.; Tang, W.; Zhu, Y. Comparison of cadmium and lead sorption by *Phyllostachys pubescens* biochar produced under a low-oxygen pyrolysis atmosphere. *Bioresour. Technol.* **2017**, *238*, 352–360. [CrossRef] [PubMed]
13. Harvey, O.R.; Herbert, B.E.; Rhue, R.D.; Kuo, L.J. Metal interactions at the biochar-water interface: Engergetics and structure-sorption relationships elucidated by flow adsorption microcalorimetry. *Environ. Sci. Technol.* **2011**, *45*, 5550–5556. [CrossRef] [PubMed]
14. Flores-Cano, J.V.; Leyva-Ramos, R.; Mendoza-Barron, J.; Guerrero-Coronado, R.M.; Aragón-Piña, A.; Labrada-Delgado, G.J. Sorption mechanism of Cd(II) from water solution onto chicken eggshell. *Appl. Surf. Sci.* **2013**, *276*, 682–690. [CrossRef]
15. Park, J.H.; Choppala, G.K.; Bolan, N.S.; Chung, J.W.; Chuasavathi, T. Biochar reduces the bioavailability and phytotoxicity of heavy metals. *Plant Soil* **2011**, *348*, 439–451. [CrossRef]
16. Wang, R.Z.; Huang, D.L.; Liu, Y.G.; Zhang, C.; Lai, C.; Zeng, G.M.; Cheng, M.; Gong, X.M.; Wan, J.; Luo, H. Investigating the adsorption behavior and the relative distribution of Cd^{2+} sorption mechanisms on biochars by different feedstock. *Bioresour. Technol.* **2018**, *261*, 265–271. [CrossRef]
17. Keiluweit, M.; Nigo, P.S.; Johnson, M.G.; Kleber, M. Dynamic molecular structure of plant biomass-derived black carbon (biochar). *Environ. Sci. Technol.* **2010**, *44*, 1247–1253. [CrossRef]
18. Cui, X.; Fang, S.; Yao, Y.; Li, T.; Ni, Q.; Yang, X.; He, Z. Potential mechanisms of cadmium removal from aqueous solution by *Canna indica* derived biochar. *Sci. Total Environ.* **2016**, *562*, 517–525. [CrossRef]
19. Mohan, D.; Kumar, H.; Sarswat, A.; Alexandre-Franco, M.; Pittman, C.U., Jr. Cadmium and lead remediation using magnetic oak wood and oak bark fast pyrolysis bio-chars. *Chem. Eng. J.* **2014**, *236*, 513–528. [CrossRef]
20. Huang, F.; Gao, L.Y.; Deng, J.H.; Chen, S.H.; Cai, K.Z. Quantitative contribution of Cd^{2+} adsorption mechanisms by chicken-manure-derived biochars. *Environ. Sci. Pollut. Res.* **2018**, *25*, 28322–28334. [CrossRef]
21. Wang, S.Y.; Tang, Y.K.; Li, K.; Mo, Y.Y.; Li, H.F.; Gu, Z.Q. Combined performance of biochar sorption and magnetic separation processes for treatment of chromium-contained electroplating wastewater. *Bioresour. Technol.* **2014**, *174*, 67–73. [CrossRef]
22. Milonjić, S.K. A consideration of the correct calculation of thermodynamic parameters of adsorption. *J. Serb. Chem. Soc.* **2007**, *72*, 1363–1367. [CrossRef]
23. Wang, Z.; Liu, G.; Zheng, H.; Li, F.; Ngo, H.H.; Guo, W.; Liu, C.; Chen, L.; Xing, B. Investigating the mechanisms of biochar's removal of lead from solution. *Bioresour. Technol.* **2015**, *177*, 308–317. [CrossRef] [PubMed]
24. Lu, H.; Zhang, W.; Yang, Y.; Huang, X.; Wang, S.; Qiu, R. Relative distribution of Pb^{2+} sorption mechanisms by sludge-derived biochar. *Water Res.* **2012**, *46*, 854–862. [CrossRef] [PubMed]
25. Cao, X.; Harris, W. Properties of dairy-manure-derived biochar pertinent to its potential use in remediation. *Bioresour. Technol.* **2010**, *101*, 5222–5228. [CrossRef] [PubMed]
26. Xu, X.; Zhao, Y.; Sima, J.; Zhao, L.; Masek, O.; Cao, X. Indispensable role of biochar-inherent mineral constituents in its environmental applications: A review. *Bioresour. Technol.* **2017**, *241*, 887–899. [CrossRef]
27. Dewage, N.B.; Liyanage, A.S.; Pittman, C.U., Jr.; Mohan, D.; Mlsna, T. Fast nitrate and fluoride adsorption and magnetic separation from water on α-Fe_2O_3 and Fe_3O_4 dispersed on Douglas fir biochar. *Bioresour. Technol.* **2018**, *263*, 258–265. [CrossRef]
28. Cao, X.; Ma, L.; Gao, B.; Harris, W. Dairy-manure derived biochar effectively sorbs lead and atrazine. *Environ. Sci. Technol.* **2009**, *43*, 3285–3291. [CrossRef]
29. Uchimiya, M.; Lima, I.M.; Thomas Klasson, K.; Chang, S.; Wartelle, L.H.; Rodgers, J.E. Immobilization of heavy metal ions (Cu^{II}, Cd^{II}, Ni^{II}, and Pb^{II}) by broiler litter-derived biochars in water and soil. *J. Agric. Food Chem.* **2010**, *58*, 5538–5544. [CrossRef]
30. Inyang, M.I.; Gao, B.; Yao, Y.; Xue, Y.; Zimmerman, A.; Mosa, A.; Pullammanappallil, P.; Ok, Y.S.; Cao, X. A review of biochar as a low-cost adsorbent for aqueous heavy metal removal. *Crit. Rev. Environ. Sci. Technol.* **2015**, *46*, 406–433. [CrossRef]
31. Li, G.Y.; Jiang, Y.R.; Huang, K.L.; Ding, P.; Chen, J. Preparation and properties of magnetic Fe_3O_4-chitosan nanoparticles. *J. Alloys Compd.* **2008**, *466*, 451–456. [CrossRef]

32. Huang, F.; Dang, Z.; Guo, C.L.; Lu, G.N.; Gu, R.R.; Liu, H.J.; Zhang, H. Biosorption of Cd(II) by live and dead cells of *Bacillus cereus* RC-1 isolated from cadmium-contaminated soil. *Colloids Surf. B* **2013**, *107*, 11–18. [CrossRef]
33. Çolak, F.; Atar, N.; Yazıcıoğlu, D.; Olgun, A. Biosorption of lead from aqueous solutions by *Bacillus* strains possessing heavy-metal resistance. *Chem. Eng. J.* **2011**, *173*, 422–428. [CrossRef]
34. Wnetrzak, R.; Leahy, J.J.; Chojnacka, K.W.; Saeid, A.; Novotny, E.; Jensen, L.S.; Kwapinski, W. Influence of pig manure biochar mineral content on Cr(III) sorption capacity. *J. Chem. Technol. Biot.* **2014**, *89*, 569–578. [CrossRef]
35. Kołodyńska, D.; Wnętrzak, R.; Leahy, J.J.; Hayes, M.H.B.; Kwapiński, W.; Hubicki, Z. Kinetic and adsorptive characterization of biochar in metal ions removal. *Chem. Eng. J.* **2012**, *197*, 295–305. [CrossRef]
36. Vijayaraghavan, V.; Yun, Y.S. Bacterial biosorbents and biosorption. *Biotechnol. Adv.* **2008**, *26*, 266–291. [CrossRef] [PubMed]
37. Harikishore Kumar Reddy, D.; Lee, S.M. Magnetic biochar composite: Facile synthesis, characterization and application for heavy metal removal. *Colloids Surf. A* **2014**, *454*, 96–103. [CrossRef]
38. Kołodyńska, D.; Krukowska, J.; Thomas, P. Comparison of sorption and desorption studies of heavy metal ions from biochar and commercial active carbon. *Chem. Eng. J.* **2017**, *307*, 353–363. [CrossRef]
39. Yahya, S.K.; Zakaria, Z.A.; Samin, J.; Santhana Raj, A.S.; Ahmad, W.A. Isotherm kinetics of Cr(III) removal by non-viable cells of *Acinetobacter haemolyticus*. *Colloids Surf. B* **2012**, *94*, 362–368. [CrossRef]
40. Kim, W.K.; Shim, T.; Kim, Y.S.; Hyun, S.; Ryu, C.; Park, Y.K.; Jung, J. Characterization of cadmium removal from aqueous solution by biochar produced from a giant Miscanthus at different pyrolytic temperatures. *Bioresour. Technol.* **2013**, *138*, 266–270. [CrossRef]
41. Agrafioti, E.; Kalderis, D.; Diamadopoulos, E. Ca and Fe modified biochars as adsorbents of arsenic and chromium in aqueous solutions. *J. Environ. Manag.* **2014**, *146*, 444–450. [CrossRef]
42. Xiao, F.; Chen, J.; Cao, W.; Yang, C.; Chen, J.; Luo, Z. Removal of heavy metals from aqueous solution using chitosan-combined magnetic biochars. *J. Colloid Interface Sci.* **2019**, *540*, 579–584. [CrossRef] [PubMed]
43. Lalhmunsiama Gupta, P.L.; Jung, H.; Tiwari, D.; Kong, S.H.; Lee, S.M. Insight into the mechanism of Cd and Pb removal by sustainable magnetic biosorbent precursor to Chlorella vulgaris. *J. Taiwan Inst. Chem. Eng.* **2017**, *71*, 206–213. [CrossRef]
44. Ali, I.; Al-Othman, Z.A.; Alwarthan, A.; Asim, M.; Khan, T.A. Removal of arsenic species from water by batch and column operations on bagasse fly ash. *Environ. Sci. Pollut. Res.* **2014**, *21*, 3218–3229. [CrossRef] [PubMed]
45. Frantz, T.S.; Silveira, N.; Quadro, M.S.; Andreazza, R.; Barcelos, A.A.; Cadaval, T.R.; Pinto, L.A. Cu(II) adsorption from copper mine water by chitosan films and the matrix effects. *Environ. Sci. Pollut. Res.* **2017**, *24*, 5908–5917. [CrossRef]
46. Huang, X.; Wei, D.; Zhang, X.; Fan, D.; Sun, X.; Du, B.; Wei, Q. Synthesis of amino-functionalized magnetic aerobic granular sludge-biochar for Pb(II) removal: Adsorption performance and mechanism studies. *Sci. Total Environ.* **2019**, *685*, 681–689. [CrossRef]
47. Zhang, F.; Wang, X.; Yin, D.; Peng, B.; Tan, C.; Liu, Y.; Wu, S. Efficiency and mechanisms of Cd removal form aqueous solution by biochar derived from water hyacinth (*Eichornia crassipes*). *J. Environ. Manag.* **2015**, *153*, 68–73. [CrossRef]
48. Demirbas, A. Effect of temperature and particle size on bio-char yield from pyrolysis of agricultural residues. *J. Anal. Appl. Pyrolysis* **2004**, *72*, 243–248. [CrossRef]
49. Xu, Y.; Chen, B. Organic carbon and inorganic silicon speciation in rice-bran-derived biochars affect its capacity to adsorb cadmium in solution. *J. Soils Sediments* **2015**, *15*, 60–70. [CrossRef]
50. Park, J.H.; Wang, J.J.; Kim, S.H.; Cho, J.S.; Kang, S.W.; Delaune, R.D.; Han, K.J.; Seo, D. Recycling of rice straw through pyrolysis and its adsorption behaviors for Cu and Zn ions in aqueous solution. *Colloids Surf. A* **2017**, *533*, 330–337. [CrossRef]
51. Xu, X.; Cao, X.; Zhao, L. Comparison of rice husk- and dairy manure-derived biochars for simultaneously removing heavy metals from aqueous solutions: Role of mineral components in biochars. *Chemosphere* **2013**, *92*, 955–961. [CrossRef]
52. Xiao, X.; Chen, B.; Zhu, L. Transformation, morphology, and dissolution of silicon and carbon in rice straw-derived biochars under different pyrolytic temperatures. *Environ. Sci. Technol.* **2014**, *48*, 3411–3419. [CrossRef] [PubMed]

53. Keiluweit, M.; Kleber, M. Molecular-level interactions in soils and sediments: The role of aromatic π-systems. *Environ. Sci. Technol.* **2009**, *43*, 3421–3429. [CrossRef] [PubMed]
54. Machida, M.T.; Mochimaru, T.; Tatsumoto, H. Lead(II) adsorption onto the graphene layer of carbonaceous materials in aqueous solution. *Carbon* **2006**, *44*, 2681–2688. [CrossRef]
55. Chen, T.; Zhou, Z.; Han, R.; Meng, R.; Wang, H.; Lu, W. Adsorption of cadmium by biochar derived from municipal sewage sludge: Impact factors and adsorption mechanism. *Chemosphere* **2015**, *134*, 286–293. [CrossRef]
56. Sun, C.; Chen, T.; Huang, Q.; Wang, J.; Lu, S.; Yan, J. Enhanced adsorption for Pb(II) and Cd(II) of magnetic rice husk biochar by $KMnO_4$ modification. *Environ. Sci. Pollut. Res.* **2019**, *26*, 8902–8913. [CrossRef]
57. Rajput, S.; Pittman, C., Jr.; Mohan, D. Magnetic magnetite (Fe_3O_4) nanoparticle synthesis and applications for lead (Pb^{2+}) and chromium (Cr^{6+}) removal from water. *J. Colloid Interface Sci.* **2016**, *468*, 334–346. [CrossRef]